Vertical Drift Chambers for the Hall A High Resolution Spectrometers at Jefferson Lab

K.G. Fissum [1], W. Bertozzi, J.P. Chen [2], D. Dale [3], J. Gao [4], S. Gilad, C.R. Leathers [5], N. Liyanage [2], J.A. Templon [6], R. Wechsler [7], J. Zhao [8]

Massachusetts Institute of Technology, Cambridge, MA 02139, USA

H.C. Fenker, A. Gavalya, R.O. Michaels, E.A.J.M Offermann [9], J. Segal, B. Wojtsekhowski

Thomas Jefferson National Accelerator Facility, Newport News, VA 23606, USA

The High Resolution Spectrometers in Hall A at Jefferson Laboratory have been instrumented with state-of-the-art Vertical Drift Chambers designed and constructed by the Nuclear Interactions Group at MITLNS in conjunction with the Physics Division at Jefferson Lab. These chambers rely on a unique, high cell-density design made possible by the absence of field-shaping wires. Each chamber has an inherent per-plane resolution for 5-cell cosmic ray tracks of 145 μm FWHM when operated on the bench at -4.8 kV with argon-isobutane gas, and 225 μm FWHM for 5-cell electron tracks when operated in the High Resolution Spectrometer detector stack at -4.0 kV with argon-ethane gas. The design and construction facilitates wire placement and replacement to 50 μm, very low dark current, and no crosstalk. The detectors have been in almost continuous use since April 1996, providing reliable, high-resolution charged-particle tracking data for the Hall A physics program.

[1] University of Lund, Box 118, SE-221 00 Lund, Sweden
[2] Thomas Jefferson National Accelerator Facility, Newport News, VA 23606, USA
[3] University of Kentucky, Lexington, KY 40506, USA
[4] California Institute of Technology, Pasadena CA 91125, USA
[5] Pennsylvania State University, University Park, PA 16802, USA
[6] University of Georgia, Athens, GA 30602, USA
[7] University of California at Santa Cruz, Santa Cruz, CA 95064, USA
[8] General Electric CRD, Schenectady, NY 12301, USA
[9] Renaissance Technologies Corporation, East Setauket, NY 11733, USA

Jefferson Lab Technical Memorandum *19 June 2000*

1 Introduction

Hall A [1] at Jefferson Laboratory [2] boasts an identical pair of 4 GeV/c superconducting spectrometers (HRS) [3]. The physics research program [4] includes precision studies of both the electromagnetic responses of hadronic systems and the momentum distributions of nucleons within nuclei. These types of experiments often require the absolute measurement of cross sections at the 1% level. Thus, strict demands were made on the design of the optical properties of the HRS. These demands included [5]:

- a FWHM momentum resolution of 1×10^{-4};
- the capability to determine particle trajectories with a FWHM resolution in the horizontal (vertical) laboratory angle of 0.5 mrad (1.0 mrad);
- a 10% momentum bite; and
- the desire to use up to a 10-cm extended target, with a FWHM target position reconstruction resolution of 1 mm.

The as-built HRS have a horizontal (vertical) acceptance of ± 28 mrad (± 60 mrad), and a focal plane that closely coincides with the laboratory horizontal plane. In the vicinity of the focal plane, the beam envelope is approximately 2.00 m in the quasi-dispersive direction by 0.20 m in the transverse direction. The nominal particle trajectory angle at the focal plane is $(45 \pm 7)^\circ$ in the spectrometer midplane. To take full advantage of this optical design, wire chambers having an inherent resolution per plane of $\sim$235 μm (FWHM) were proposed for particle tracking [6].

In this article, we present an overview of the Jefferson Laboratory Hall A wire chamber project. We start by outlining the major design considerations and the construction in general. Next, we present an overview of routine operations, and discuss the resulting inherent performance. We then illustrate in detail how we use the chambers for particle tracking. And finally, we profile our overall operating experience.

2 Design considerations

Vertical Drift Chambers (VDCs) [7–9] were chosen to instrument the HRS. A dual-VDC system was constructed for each spectrometer (see Fig. 1). A lower VDC is positioned to coincide as much as possible with the spectrometer focal plane, and a second VDC is located above it to enable precise angular reconstruction of particle trajectories. Note that the shape of the focal plane is complex, and does not coincide exactly with the lower VDC. The vertical separation between like wire planes is 0.335 m.

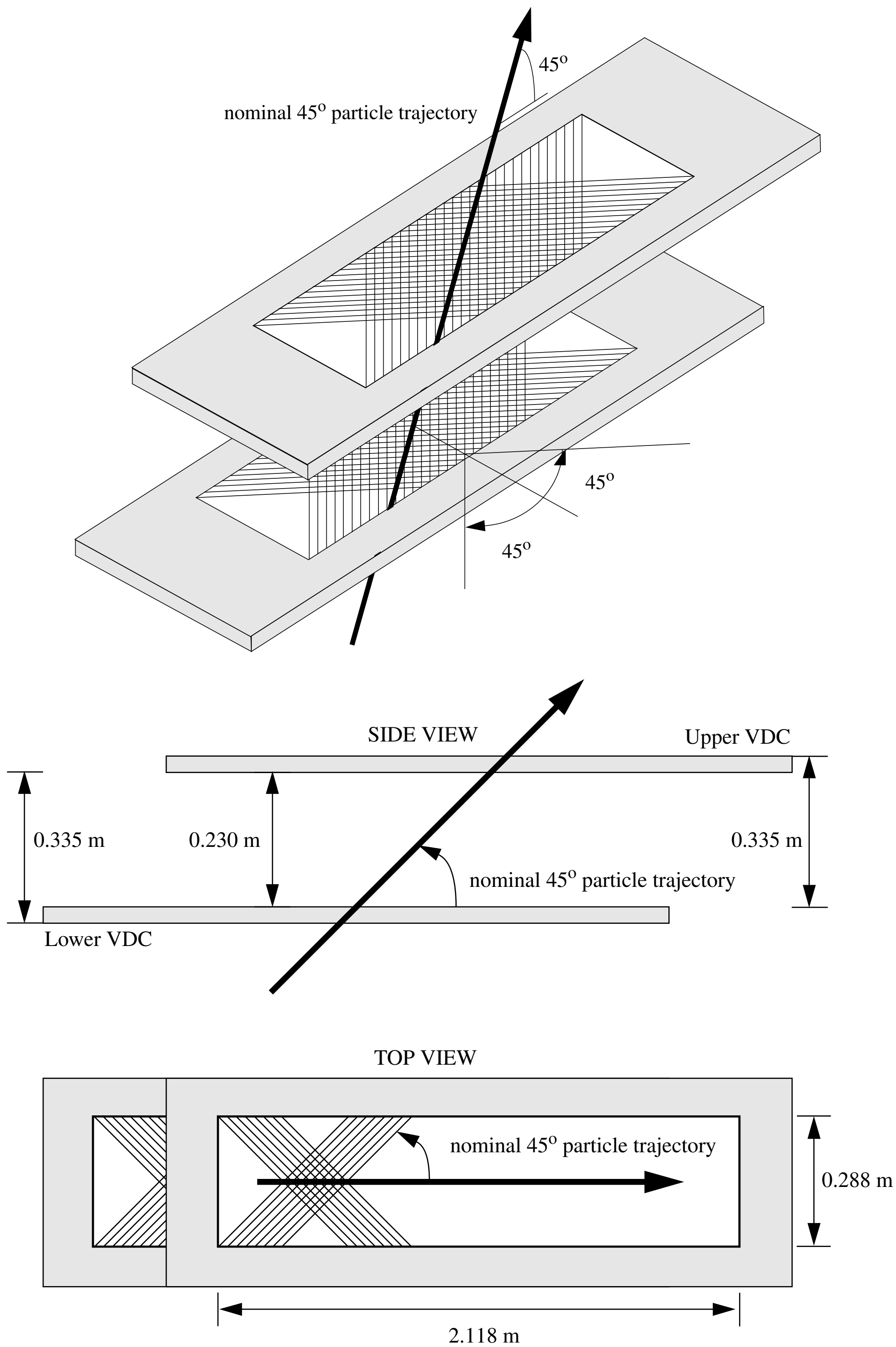

Fig. 1. Schematic layout of the VDCs (not to scale). The rectangular area of each wire frame aperture is 2.118 m × 0.288 m (see 3.2.1). The U and V sense wires are orthogonal to each other and lie in the horizontal plane of the laboratory. They are inclined at an angle of 45° with respect to both the dispersive and non-dispersive directions. The lower VDC coincides (essentially) with the spectrometer focal plane. The vertical offset between like wire planes is 0.335 m.

A reliable and convenient UV sense-wire configuration was selected for the VDCs. The U and V sense wires are orthogonal to each other and lie in the horizontal plane of the laboratory. They are inclined at an angle of 45° with respect to the dispersive and non-dispersive directions (see Fig. 1). A new and important feature of these VDCs is that there are no field-shaping (guard) wires (see 3.2). They are thus approximately three times thinner than similar VDCs with two guard wires per sense wire would have been, which reduces multiple scattering and operating voltage. The wires themselves are individually mounted and positioned, a technique originally developed at SLAC [10], and subsequently adopted and extensively modified by several groups at MITLNS [11]. This greatly reduces the workload associated with replacing one should it break.

As wire chambers form the core of any tracking package, their dependable operation is of critical importance. Since dependability and regular maintenance go hand-in-hand, ease of serviceability was a major design consideration. Thus, a "swap-in/swap-out" modularity is employed wherever possible in the design. Further, since the VDCs represent a substantial investment of money, time, and manpower, it is clearly very important to construct and use them in a manner that maximizes the mean time between failures [12]. To this end, electrical noise is minimized by choosing conductive components with little secondary ion emission. Minimizing operating voltage and eliminating severe geometry such as sharp edges from the design avoids breakdowns, and reduces the rate at which contaminants electrodeposit onto the sense wire surfaces, destroying their sensitivity to ionization. Well-configured armor for the tracking package is used to reduce the possibility of window rupture or wire breakage. And finally, the chamber interiors are kept clean by constantly flushing them with gas.

3 Construction

3.1 Chassis

A cross-sectional schematic view (not to scale) of a VDC is shown in Fig. 2.

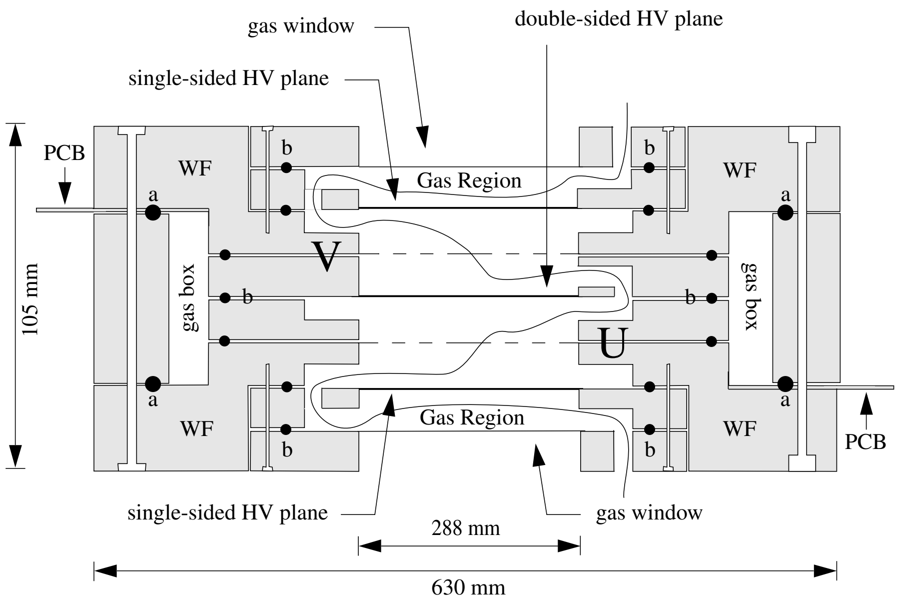

Fig. 2. Cross-sectional schematic view of the VDC (not to scale). Wire frames are labelled ‘WF’, while ‘PCB’ indicates the printed circuit boards used for relaying the signals from the wires to the preamp/discriminator cards. These cards are mounted on the circuit boards. The nominal path of the gas flow is indicated by the meandering line. The dashed lines indicate the location of the U- and V-wire planes. Two types of O-ring seals (indicated by the solid black circles) are located at points ‘a’ and ‘b’. Bolt channels are indicated in the vicinity of the type ‘a’ O-rings, while tap channels are shown in the vicinity of the type ‘b’ O-rings. Gas flows first through the chamber, and then is channeled through the gas box before being exhausted.

The dielectric material Stesalit 4411W [13] (an epoxy/glass-fiber composite) machined to a uniform planarity of ± 0.05 mm with a thickness tolerance of ± 0.1 mm is used as the base material for the VDC frames. This material was chosen because its glass fibers are very small and randomly oriented, so that precision machining (50-μm allowance on standard milling equipment) is possible without inducing flaking or chafing.

All outside surfaces of the Stesalit frames are plated with a 70-μm thick layer of copper to suppress RF pickup and static charge buildup. Further, after assembly, the entire chassis is covered with an outer sheathing of 125-μm thick copper. The individual copper plates forming this sheath are electrically connected with conductive copper tape.

3.2 Sense region

A new feature of these VDCs is that there are no guard wires. Guard wires are commonly used to make the electric field in the drift region more uniform, and to reduce cross talk between adjacent drift cells. They are generally located in the plane of and in between the sense wires, and are held at ground potential [8,9]. Since they create, in essence, inactive drift cells, they increase the overall chamber thickness needed for a given number of cells to be traversed by a particle track. This, in turn, results in a higher operating voltage for a given average field. In the humid coastal Virginia climate, a moderate operating voltage is prudent.

Fig. 3 shows a cross section of the sense region for a single wire plane.

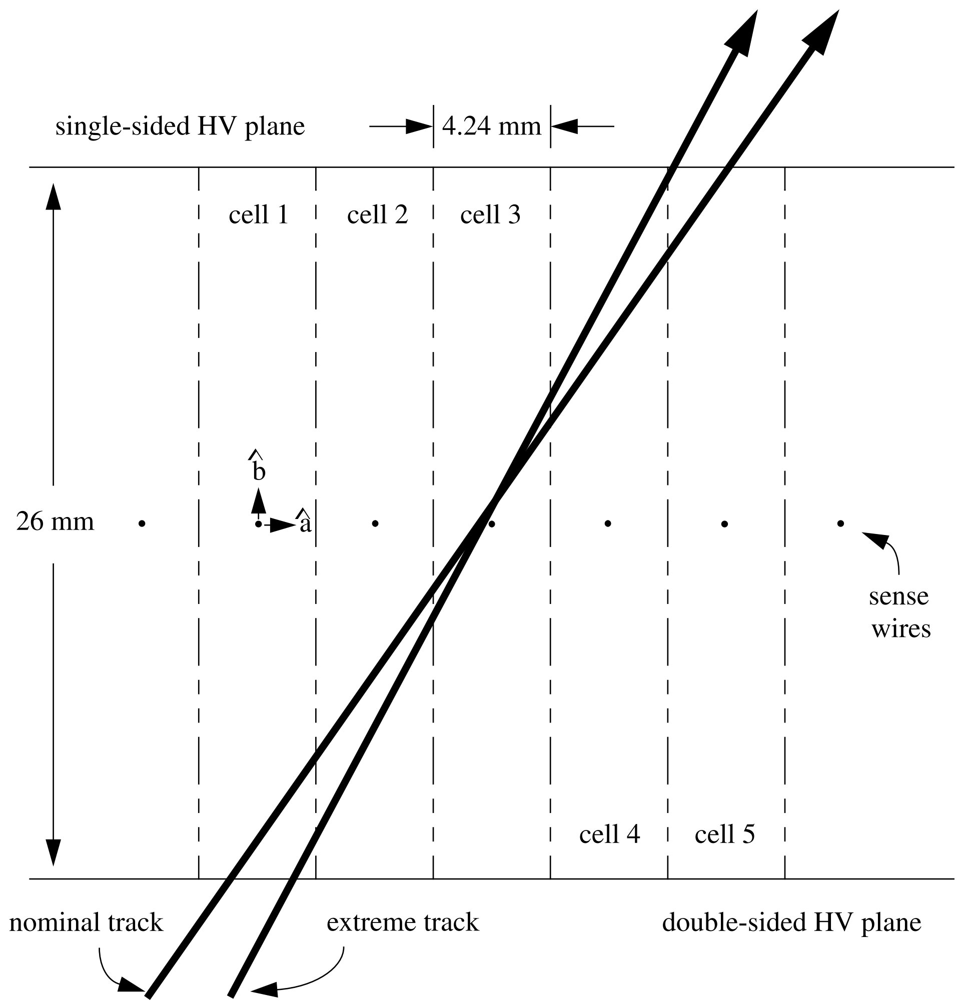

Fig. 3. Cross-sectional view of the sense region for a single wire plane. The wires are perpendicular to the page and are connected to ground. The dashed lines delineate the drift cells. A nominal (extreme) track with a lab angle of 45° (52°) has an angle of 55° (62°) in this coordinate system.

The design goal for these wire chambers was to have nominal (maximum) trajectories cross five (three) drift cells. The nominal (maximum) trajectory angle for the HRS in the spectrometer midplane is 45° (52°). Given the orientation of the wires with respect to the spectrometer midplane (see Fig. 1), these angles correspond to angles of 55° (62°) in a plane perpendicular to the sense wires. As shown in Fig. 3, for a wire chamber with no inactive drift cells, a cell height of 26 mm and a cell width of 4.24 mm (corresponding to a wire separation of 6 mm in the spectrometer midplane) is sufficient to accomplish the design goal. This cell width is also large enough to ensure the capacitance necessary for the generation of acceptable signals.

These VDCs accomodate fields on the order of 0.3 kV/mm with a cathode-anode distance of 13 mm. The tradeoff is a slight increase in the complexity of the track reconstruction algorithm, and a very thin region of indistinct electric field at the boundary between two drift cells. `GARFIELD` models [14,15] of the magnitude of the equipotential surfaces and the magnitude of the electric field for the VDC sense region are shown in Figs. 4 and 5.

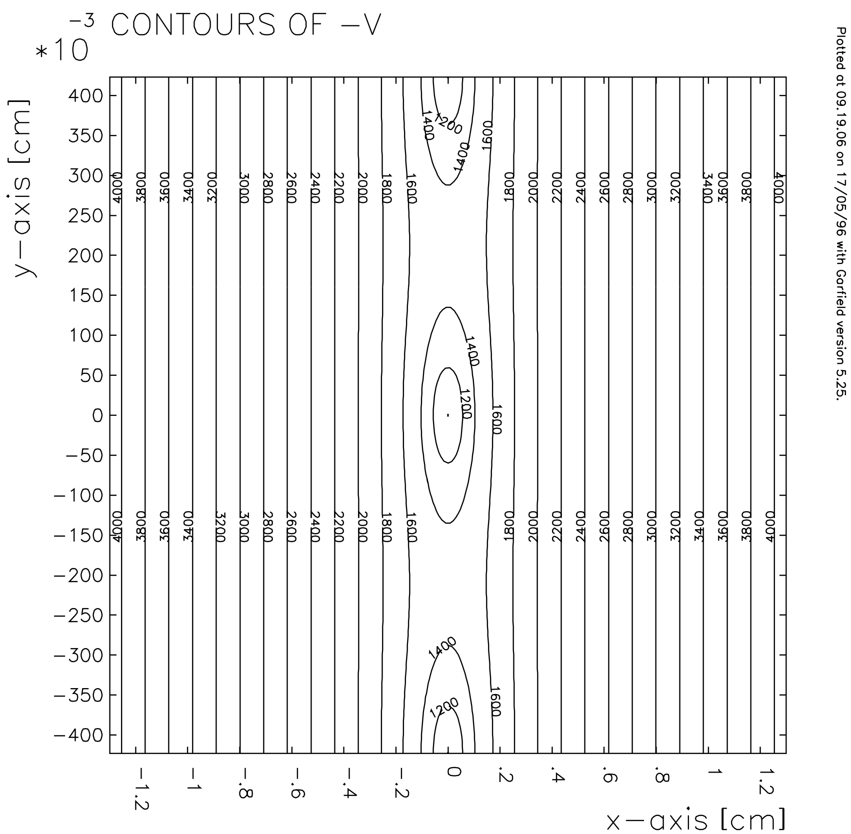

Fig. 4. Temporary - waiting on a new figure from Templon. `GARFIELD` model [14,15] of the equipotential surfaces in the vicinity of a drift cell. See Fig. 3 for the definition of the coordinates. In the region close to the sense wire, the equipotential surfaces undergo a transition from parallel to elliptical.

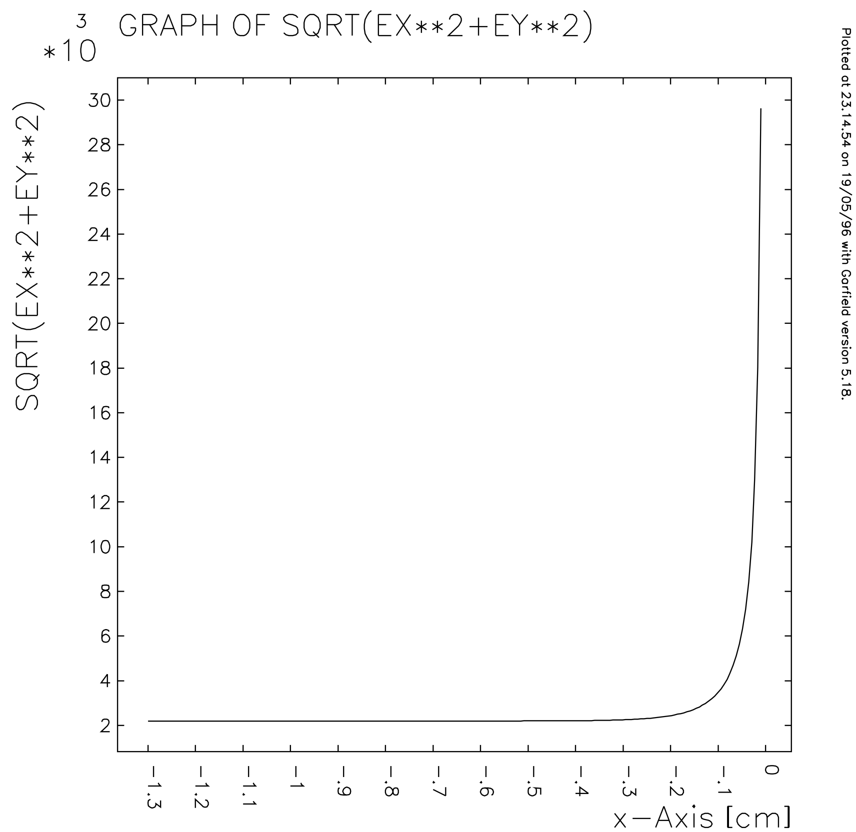

Fig. 5. Temporary - waiting on a new figure from Templon. `GARFIELD` model [14,15] of the magnitude of the electric field as a function of distance from the sense wire in the direction perpendicular to the wire. See Fig. 3 for the definition of the coordinates. Over the majority of the drift cell, the electric field is constant, and has a magnitude less than 0.3 kV/mm.

3.2.1 Wire frames

Geometrical considerations and the desire to have four identical VDCs led to the choice of rectangular apertures for the wire frames of length 2.118 m and width 0.288 m. The wire frames are labelled 'WF' in Fig. 2. They were designed with a symmetric configuration to reduce costs, since a single shape could be used for both the U- and V-planes by simply flipping it upside-down. All wire planes lie in the horizontal plane of the laboratory. The lengths and tensions of the U- and V-wires are the same, which results in a matched inherent resolution on all planes. The wires are mounted individually in slots. The slots are machined to a tolerance of ± 10 μm to ensure that they are parallel, evenly spaced, and set to a uniform depth in the frame.

A detailed description of the wire-mounting procedure may be found in [16,17]. A short overview is presented here. Note that while labor-intensive, this wire-mounting scheme makes precision wire placement possible without a complex and expensive stringing machine. Further, should a wire break, the workload associated with repairing it is greatly reduced, and its replacement may be positioned with the same accuracy as the original.

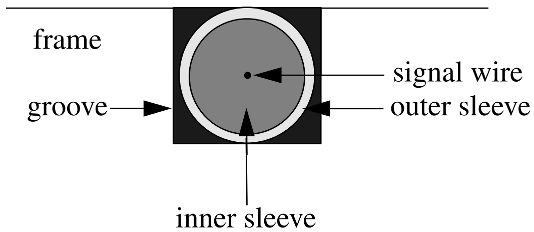

Fig. 6. A cross-sectional view of a single wire fixture (not to scale). The outer sleeve is permanently attached with epoxy within the milled rectangular channel. The inner sleeve is attached to the wire using an air-driven crimping tool. The seal between the two sleeves is not gas-tight.

Fig. 6 shows a cross-sectional view of a single wire in its positioning channel (not to scale). The wire is drawn by hand through a very small (100-μm diameter) hole in a precision inner sleeve. An air-driven crimping tool is used to attach the inner sleeve to the wire. This inner sleeve is set by hand within an outer sleeve which has been positioned within a groove in the frame. Both types of sleeves were manufactured from 20304 SMLS stainless steel using a precision extrusion process, and subsequently annealed.

Table 1
Sleeve dimensions and tolerances.

Sleeve	length (±0.050”)	inner diameter (±0.0005”)	outer diameter (±0.0005”)
outer	1.100	0.0405	0.0700
inner	1.250	0.0040	0.0390

As shown in Fig. 7, the outer sleeves extend about 10 mm past the edge of the frame. The glue used to attach the outer sleeve to the wire frames is a two-component product from CIBA [18], which combines resin (Araldite AW116) and hardener (HV 953U). Since this epoxy is the same as that in the Stesalit frame, the outer sleeve is permanently embedded within the wire frame once the epoxy cures. Any excess glue protruding above the surface of the frame is machined smooth, so that the surface of the wire frame is flat and square.

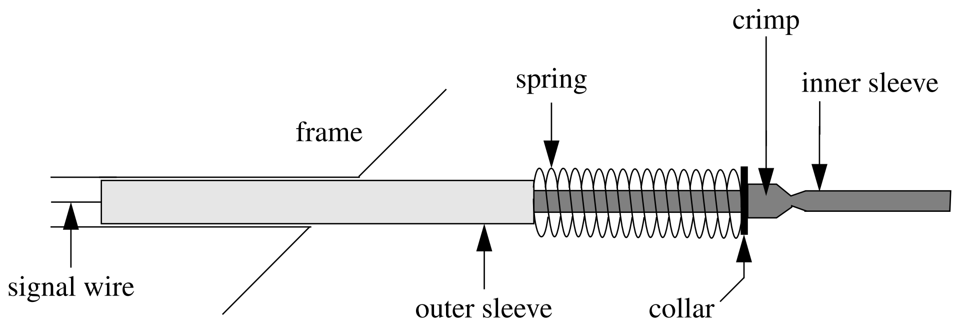

Fig. 7. The spring-loaded end of a single wire (not to scale). The outer sleeve, which is permanently attached to the frame, extends about 10 mm into the gas box. The inner sleeve is free to slide telescopically within the outer sleeve, subject to the constraint of the spring, collar, and crimp.

A uniform tension of about 0.7 N is applied to the wires using a pulley, a spring, and a 70-g mass. As shown in Fig. 7, collars maintain the resulting position of the inner sleeves with respect to the outer sleeves. In this manner, the inner sleeve is left free to slide telescopically within the fixed outer sleeve. This degree-of-freedom is important since it reduces the brittleness of the wire assembly by allowing some play should an unforeseen mechanical or electrostatic strain on the wire arise. However, the resulting seal between the two sleeves is not gas-tight.

While this results in wire frames which are mechanically stressed by the wires they support, it is desirable since the signal wire is held firmly at the center of its slot, and is unable to sag. This is very important for three reasons:

- sharp physical configuration changes where the wire crosses the boundary between the sense-region and the wire frame are eliminated, as the wire is isolated from the frame by the gas in the slot in which it sits;
- the mounting apparatus associated with positioning the wire is kept away from the sense region; and
- the parallel wires form a uniform, rectilinear plane, even under the influence of a strong electric field.

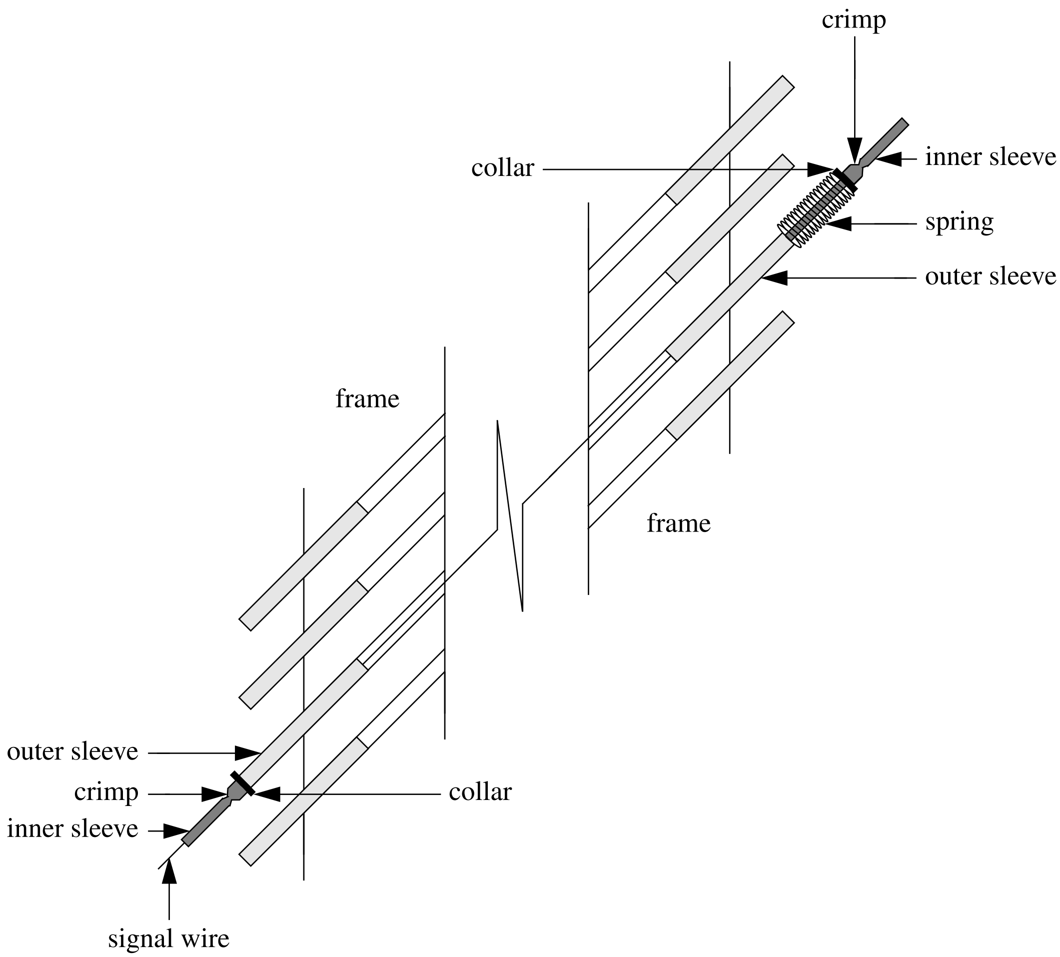

Fig. 8. An overview of a wireframe (not to scale). The tension in the wire is maintained using a spring and collar. Each signal wire sits in a gas-filled channel so that it is isolated from the boundary between the sense region and the wire frame.

After the installation of all the wires on a given frame was completed, the wire positioning was checked on a precision optical bench and found to be better than ± 50 μm for each wire. Since this is a random misalignment and five cells in general contribute to a particle track, the maximum degradation of the reconstruction algorithm resolution due to wire misplacement is less than ± 25 μm.

3.2.2 Printed circuit boards

The signal wires are connected via small hand-soldered jumpers to large area printed circuit boards (labelled 'PCB' in Fig. 2). They relay the signals to 16-conductor cable connectors via conductive strips. All non-critical surfaces of the copper-backed circuit boards are plated with solder to form a ground plane. Fine thickness tolerances were required at the point where the circuit board contacted the gas box to keep the entire chassis square and gas-tight when completely assembled. For this reason, a strip on the printed circuit board which comes in contact with the gas box was first "built up" using a material of the same type, and then machined to the correct thickness and planarity. The circuit boards are segmented to facilitate their production. Conductive bridges have been soldered between like circuit elements on adjacent boards. This ensures good electrical contact across the boundaries.

3.2.3 Wires

There are 400 wires in each wire plane.

The sense-wire portion of each wire plane consists of 368 type Luma 861/60, 20-μm diameter, 4% gold-plated tungsten (with a 3% rhenium additive to reduce brittleness) wires of straightness grade 1 and less than 5% ovality [19]. Tungsten is used as the base material for the wires because it has a very high tensile strength. Gold is used as the conductive plating because it is resistant to corrosion and has a high work function (which reduces secondary emission at the conductive surface). The total length of each of the sense wires which span the width of the chamber aperture and connect to the printed circuit board is approximately 60 cm.

The first 16 wires at each end of a wire plane are grounded for field-shaping purposes. These 32 grounded wires have gradually increasing diameters (from 20 μm to 100 μm) and decreasing lengths (from 60 cm to 20 cm) as the corner of the wire frame is approached. This reduces the electric field in the vicinity of the wires and thus acts to suppress spontaneous discharge. It also reduces the leakage current.

3.3 Windows

Two distinct types of windows are used in the VDCs - high voltage (HV) windows and gas windows. In both cases, Mylar was chosen as the backing material because it is strong and inexpensive. The windows have been installed in as flat and uniform a manner as possible by stretching them taut before permanently attaching them to the frames using the two-component epoxy discussed in 3.2.1. Flat HV windows help make the electric field uniform. Subsequent to the epoxy curing, any local irregularities in the windows were removed using a heat gun.

3.3.1 HV windows

Two types of HV windows were used: single-sided gold-plated Mylar and double-sided gold-plated Mylar, both 6-μm thick. The thickness of the gold plating is (850±50) Å, for a resistance of 0.287 Ω/square. The double-sided gold-plated Mylar window acts as a central, shared cathode. In each VDC, it is located exactly in between the U- and V-wire planes, 13 mm from each of them. The two single-sided gold-plated Mylar windows are located on opposite sides of this central cathode, 26 mm from it. Together, these three HV windows define two independent regions of high voltage - one for the U-wire plane and one for the V-wire plane. A wire line is connected to each HV window via a brass tap. These three well-insulated HV-lines span the gas box and pass through the Stesalit chassis via three separately tapped channels. They are in turn soldered onto standard SHV connectors mounted on the exterior of the chassis.

3.3.2 Gas windows

The gas windows consist of 6-μm thick Mylar coated with a very thin layer of aluminum. They are grounded to the copper-plated chassis using conductive epoxy and thin brass strips. The aluminum prevents fast diffusion of moisture from the experiment Hall to the inside of the chamber.

3.4 Sealing

The entire VDC is sealed. This is because the chamber gas is flammable, so maintaining control over the containment volume enables safe operation.

3.4.1 Gas box

The sense area of a chamber sits in a large gas containment volume, including the regions labelled ‘gas box’ and the regions between the single-sided HV planes and the gas windows shown in Fig. 2. There are four distinct advantages to this design:

– the containment volume ensures that both the HV windows and all the inner chamber seals are not exposed to varying atmospheric composition and pressure, but rather a steady-state volume of dry gas of constant composition and pressure;
– gas which leaks through the sleeves which position the wires in the wire frames is contained and controlled;

– the VDC may be sealed in a multi-tiered manner, with seals associated with the window components made using seven smaller diameter O-rings located at the points labelled ‘b’, and seals associated with the gas box made using two larger diameter O-rings located at the points labelled ‘a’ (see Fig. 2); and
– the geometrical integrity of the chamber is ensured by uniformly distributing the forces associated with tightening the bolts used to compress the large O-rings associated with the gas box over a square and rigid body, thus preventing any overtightening which could twist or warp the frames.

3.4.2 O-rings

The sealing between the Stesalit frame components is performed with Viton O-rings [20]. Two diameters of O-rings are used: 2.62 mm low durometer for the primary gas seal, and 4.83 mm standard durometer for the secondary gas seal.

Compressive force is exerted on the low-durometer O-rings which form the primary gas seal with a series of $\frac{1}{4}'' - 20 \times 1''$ nylon bolts inserted into holes tapped into the Stesalit window frames approximately every 9 cm (see ‘b’ in Fig. 2). Non-conductive nylon bolts were chosen due to the close proximity of the HV planes. A standard diagonal torquing sequence is used, and the bolts are tightened until they audibly protest.

Compressive force is exerted on the two O-rings which form the secondary gas seal with a series of $\frac{1}{4}'' - 20 \times 4''$ zinc-plated stainless-steel shoulder bolts inserted into holes tapped into the Stesalit gas box frames approximately every 10.5 cm (see ‘a’ in Fig. 2). Stainless steel bolts were chosen because there is no HV in the vicinity, and the gas seal at these O-rings must be very tight. Again, a standard diagonal torquing sequence, this time to 6.22 N-m, is used.

3.5 Mounting frame

Because the Stesalit VDC chassis themselves are not rigid, the VDCs are bolted to a pair of robust aluminum U-channels roughly 1 cm thick × 8 cm deep × 23 cm wide for support. The U-channels are oriented such that the 23-cm long dimension is in the laboratory vertical, and the copper-sheathed chambers are attached to the 8-cm legs (one VDC is set atop, and the other VDC is hung below). The relative positions of the two VDCs are offset by approximately 0.335 m along the length of the cartridge such that the central ray of the spectrometer nominally passes through the center of each. The channels are bolted to thick aluminum endcaps, which complete the rigid support structure (see Fig. 9). On the bottom of each of the endcaps, a pair of low-friction, precision sliding bushings are attached. These bushings are essentially hollow cylinders which have been cut in half along their symmetry axis, and allow the entire mounting frame to be set upon and slid along a pair of parallel positioning support rails.

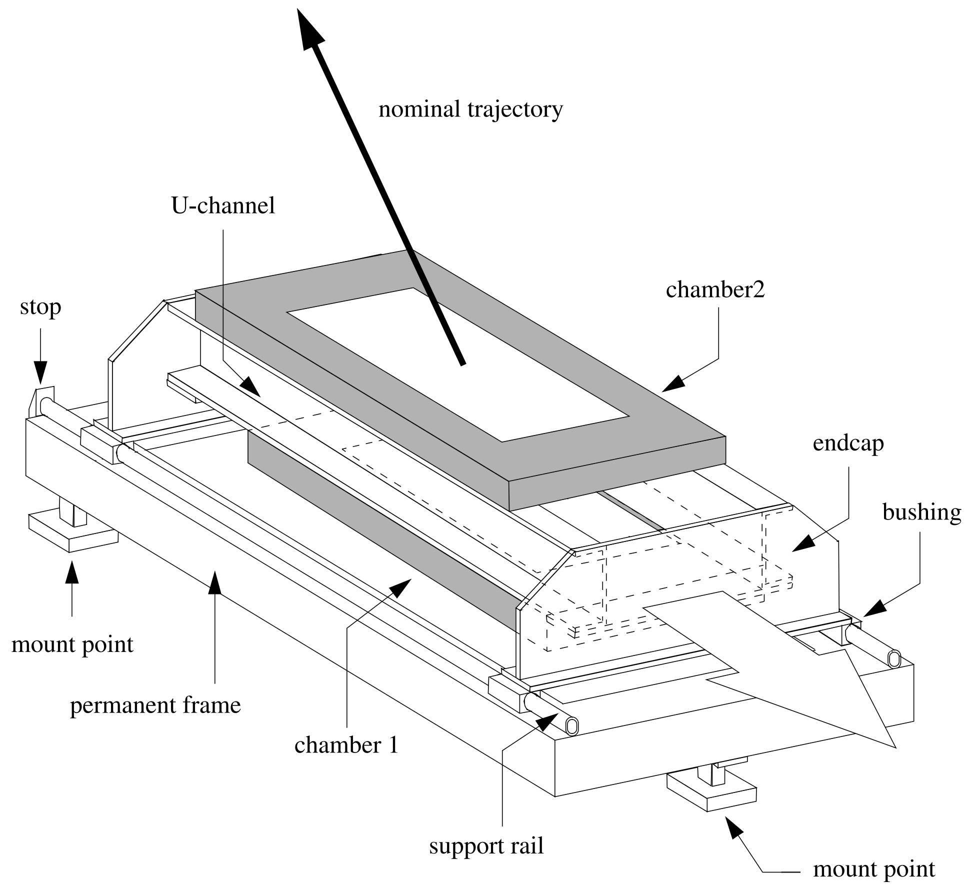

Fig. 9. The mounting frame (not to scale). The VDCs are attached to heavy aluminum U-channels in an offset configuration. A nominal trajectory is indicated. The entire cartridge may removed from its location by sliding it off the support rails.

Subsequent to the assembly of the cartridge, the VDCs are surveyed to check that they have been positioned in a square and coplanar manner. Any necessary minor adjustments are made with thin metal shims. Thus, the entire VDC cartridge retains its relative configuration at all times, even when it is removed from the spectrometer hut.

3.6 Cage

The mounting frame and VDC assembly shown in Fig. 9 is enclosed within a rectangular shell. This shell provides physical protection for the preamp/-discriminator cards which attach to the printed circuit boards located along the sides of the VDCs. It also acts as an RF shield against the large amplitude output signals generated by the cards and by standard electronics mounted in close proximity. The upper and lower face plates are made from 1.5-mm thick aluminum, and are 110 cm $\times$ 310 cm, with a 0.30 m $\times$ 2.14 m rectangular section removed from the center corresponding to the active area of the chambers. This gap is covered with 25-μm thick aluminum foil which maintains the RF shield while minimizing multiple scattering of the particles passing through it. The foil is attached to the 1.5-mm plate with conductive copper tape. The face plates are mounted one above the top VDC and one below the bottom VDC. The side panels are U-shaped, roughly 1.5-mm thick $\times$ 1-cm deep $\times$ 45-cm in height. They are constructed in 40-cm wide sections and are mounted such that the 1-cm lips attach to the upper and lower face plates. The panels complete the cage, and further confine a volume for the forced-air cooling of the cards. Connection between the side panels and the upper and lower face plates is made with adjustable clamps. The geometry is shown in Fig. 10.

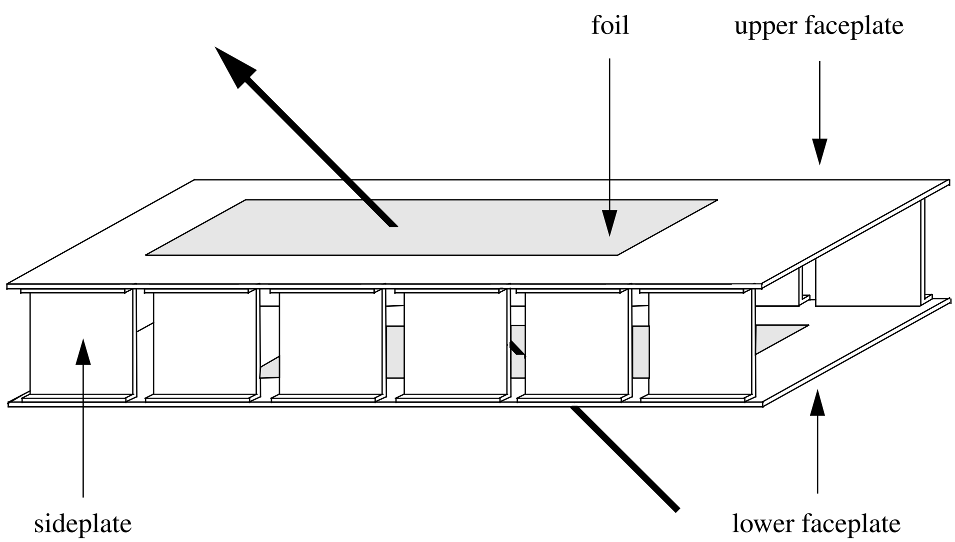

Fig. 10. The cage (not to scale). Upper and lower faceplates are separated by side plates, all made from 1.5-mm thick aluminum. The shaded areas indicate the region through which particles pass, and are covered with 25-μm thick aluminum foil. This shell is bolted around the mounting frame and VDC assembly, not shown in this sketch. A nominal trajectory is indicated.

3.7 Rails

Stainless steel support rail frames are used to transport and position the VDC apparatus. Two types of rail frames are used: fixed and portable. Fixed support rails are bolted to a heavy-duty steel frame which is permanently mounted in the spectrometer hut (see Fig. 9). Portable support rails are bolted to a frame identical in all aspects to the fixed frame, but mounted on wheels and having connection points for U-bolts so that a crane may be used to raise and lower the rail frame (with or without the VDC assembly aboard) to and from the floor of the Hall. The rails of the portable frame precisely mate to the rails of the permanent frame in the spectrometer detector hut. The VDCs may be transferred to their location in the detector hut by connecting the two sets of rails and sliding the package from one frame to the other.

Since the VDCs are removable, it is crucial that they can be returned to their exact previous location, both reliably and routinely. This is because the parametrization of the matrix elements describing the optical properties of the spectrometers is sensitive to the positioning of the VDCs [21]. Thus, the wire chamber cartridge is bolted to a pair of hard stops welded in place on the permanent frame. Positioning reproducibility of the VDC cartridge is good to ± 0.5 mm.

4 Operation

Operation of the VDCs requires four independent subsystems - gas, high voltage, low voltage and threshold, and readout.

4.1 Chamber gas

Chamber gas is provided by the Hall A Wire-chamber Gas System (HAWGS), a system based on a commercial gas controller [22]. Air Products UHP/ZERO grade Argon (99.999% pure) and CP grade ethane (99.0% pure) [23] are supplied by high pressure bottles and combined 50%/50% by volume (62%/38% by weight). This mixture is first bubbled through a constant temperature (0° C) bath of ethanol, a standard chamber gas additive which increases chamber lifetime [24]. The mixture is then distributed to each spectrometer independently. For each spectrometer, the gas is also supplied to each VDC independently. An upstream bypass bubbler filled with a 10-mm column of mineral oil allows gas to vent in overpressure situations. As shown in Fig. 2, the gas flow within each VDC is serial, with the gas first entering the U-plane volume, and subsequently exiting the V-plane volume. The gas then flows through the gas containment box. Typically, 10 ℓ/hr is supplied to a VDC. Given the VDC volume of about 30 ℓ and a leak rate that does not exceed 3 ℓ/hr, this results in a controlled gas exchange every four or five hours. This continuous flushing of chamber gas removes contaminants such as oxygen and moisture and ensures a clean, homogeneous gas supply in the sense region. This, in turn, leads to a constant, stable ionization drift velocity (see 6.4). After passing through the chambers, the gas mixture proceeds through a downstream bubbler filled with a 5-mm column of mineral oil and is vented.

4.2 High voltage (HV)

High voltage is provided to each VDC by a single channel of a Bertan 377N HV power supply [25]. These supplies sit in the spectrometer detector huts and are controlled remotely from the Counting House. The connection from the power supply to the VDC is made via standard SHV connectors mounted on RG59/U HV cable. At the VDC, the HV line is split into three parallel lines, one for each of the HV planes. This allows HV to be applied independently to each plane if needed. Note that a 10 MΩ protective resistor is placed in series with each HV plane. The HV lines are connected to the HV planes through hand-tapped tunnels in the Stesalit frames. Several layers of insulating heat shrink coating applied to the HV lines prevents arcs within the tunnels. Nominal operating voltage is -4 kV for the standard argon-ethane gas used. Typical dark current draw for cosmic rays in this configuration is $\leq$ 30 nA per VDC. Electrical stability at this relatively low operating voltage is excellent (see 7.1).

4.3 Low voltage (LV) and threshold

Forty-six 16-channel LeCroy 2735DC preamp/discriminator cards [26] are used to process signals from each VDC. A Kepco ATE 6-100m preamp power supply [27] provides +5.0 V (0.25 A) and -5.2 V (0.50 A) nominal preamp voltage (current drawn per card). A Kepco ATE 15-3m discriminator power supply [27] provides +3.0 V (4.5 mA) nominal threshold voltage (current drawn per card). The cards are actively cooled by (12 V DC) high volume fans installed in a push/pull configuration such that air is continuously drawn across them.

4.4 Readout system

The analog signals progress along signal lines on the circuit boards to the preamp/discriminator cards. At the cards, the signals are first preamplified and then discriminated. The nominal +3.0 V discriminator threshold corresponds to roughly 5 μA. From the cards, the logic signals are sent to LeCroy 1877 multihit Fastbus TDCs [26], via 16-conductor, twisted-pair ribbon cables. These cables are approximately 10-m long, and have clip-on ferrites located downstream of the preamp/discriminator cards to filter high-frequency noise. There is one TDC channel with 0.5 ns/channel resolution for each sense wire.

The sense-wire signals start the TDCs, and a common stop is provided by the event trigger. The TDC modules reside in a Kinetic Systems F050 Fastbus crate [28] which utilizes a BiRa FB8189-4 power supply [29]. The crate is interfaced to the DAQ computer.

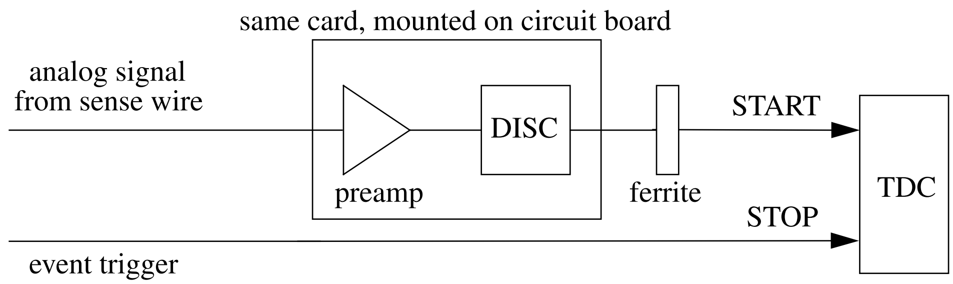

Fig. 11. A block diagram of the sense wire electronics. The preamp/discriminator cards are mounted on the circuit boards. Signals proceed to the TDCs via 10-m long, twisted-pair cables. Each wire has its own TDC channel. The TDCs have 0.5 ns/channel resolution and are operated in common stop mode.

5 Inherent performance

Data are typically used to quantify and monitor the inherent VDC characteristics during experiments. Those presented in this section were collected in typical operating mode with the VDCs mounted in the detector stack, using the standard argon-ethane gas, LV, preamp/discriminator thresholds, and HV. The following estimations of the wire efficiency and time resolution are typically calculated on a run-by-run basis and used for online monitoring of the chambers during normal operation. Note that in the following discussion, only 5-cell events are considered.

5.1 Wire efficiency

The algorithm used to estimate and track the wire efficiency is straightforward. For every event, each wire along a given wire plane is scanned. Events are identified where two sense wires fired, and there is a third sense wire between them. If the third sense wire also fired, the event is defined to be efficient for this third wire. If the third sense wire did not fire, the event is defined to be inefficient for this wire. The efficiency profile for the wire plane is obtained by evaluating

$$\epsilon = \frac{\kappa}{\kappa + \lambda} \tag{1}$$

for every wire, where κ is the number of times a wire is found to be efficient and λ is the number of times a wire is found to be inefficient. As can be seen in Fig. 12, the single wire efficiency of these chambers is better than 99%. Note that a typical track in a VDC involves from four to six wires, so that the per-track efficiency of the chambers is essentially 100%.

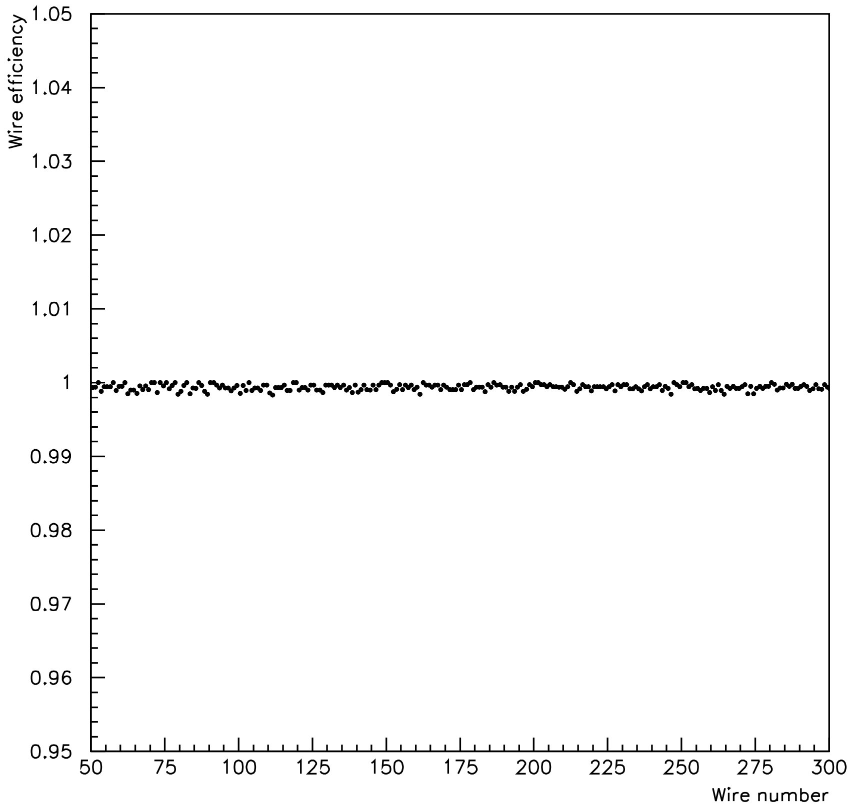

Fig. 12. Typical wire efficiency as a function of wire number for wire plane U1.

5.2 Time resolution

The algorithm used to estimate and track the inherent time resolution is also straightforward. The minimum time for the ionization electrons produced in each drift cell to drift along the electric field lines to the respective sense wires is t_i, where $i = 1, ..., 5$ for a 5-cell event. For the present discussion, the wire nearest to the point where the trajectory crosses the wire plane (wire 3 in Fig. 14) is ignored since timing signals from it require a more complex algorithm to understand and do not affect the overall resolution (see 6.2). A relative timing is then defined according to

$$\Delta T = |(t_1 - t_2) - (t_5 - t_4)|. \tag{2}$$

Fig. 13 shows the relative timing ΔT measured for a sample of 5-cell events.

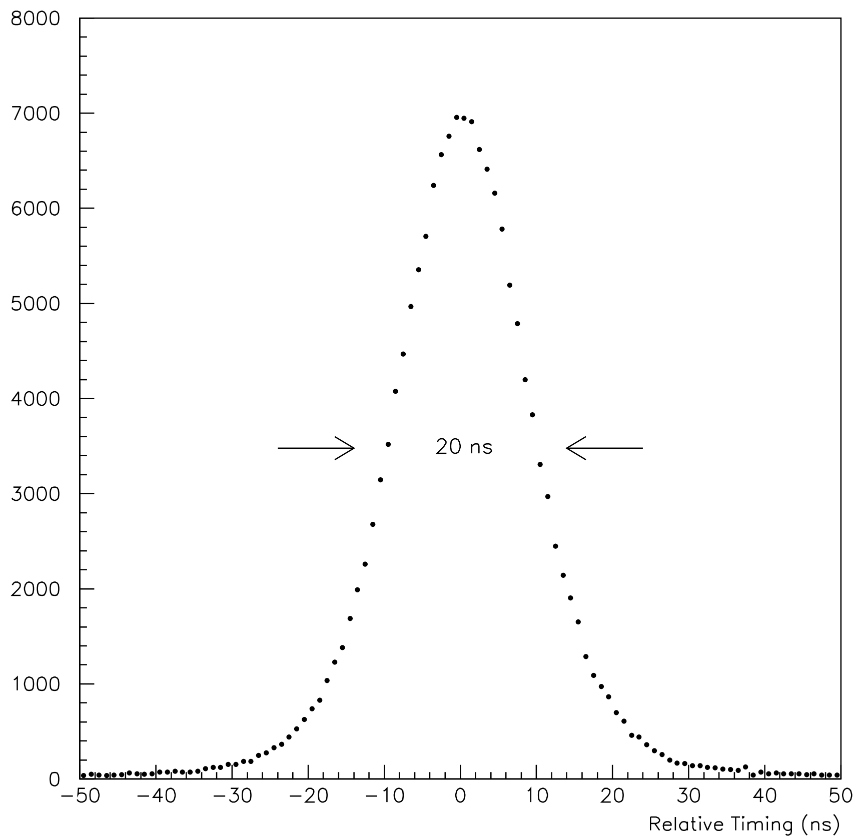

Fig. 13. The relative timing of 5-cell events (see Eqn. 2 for the definition of the relative time). The FWHM value of approximately 20 ns is indicated.

For a perfect chamber with infinitessimal resolution, this relative timing distribution would be a δ-function centered at $\Delta T = 0$. Here, the 20-ns FWHM of the distribution sets the upper limit on Δt, the inherent time resolution for a single cell in a given VDC plane. According to Eqn. 2, timing information from four TDCs connected to signal wires pairwise adjacent to the wire plane cross-over point is folded into each event in this distribution. Thus, assuming equal contributions to the total width from each of the five drift cells traversed, the per-plane FWHM time resolution is given by

$$\Delta t = \frac{1}{\sqrt{5}} \left(\frac{1}{\sqrt{4}} \cdot 20 \text{ ns} \right) = 4.5 \text{ ns}. \tag{3}$$

This value, together with the average ionization drift velocity taken from Table 2 (see 6.4), yields a measured upper limit on the per-plane FWHM position resolution for the VDCs of approximately 225 μm.

6 Track reconstruction

6.1 Overview

The data supplied by the VDCs are used to reconstruct particle trajectories. Consider Fig. 14.

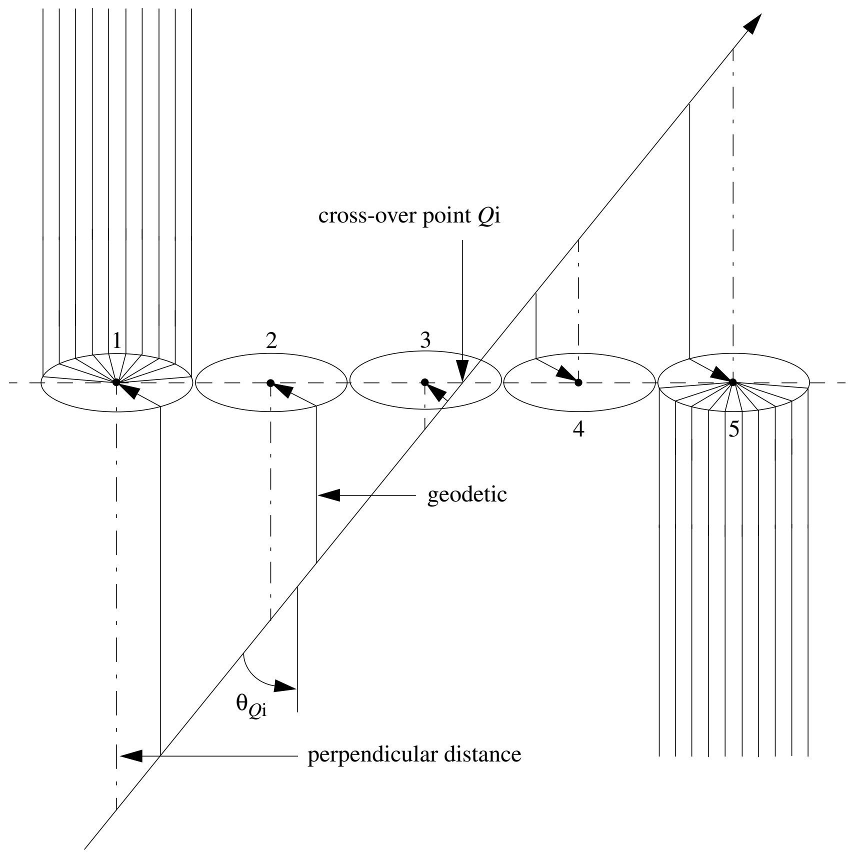

Fig. 14. A typical track resulting in a 5-cell event. The arrowed lines are paths of least time for the ionization electrons to travel from the trajectory to the sense wires. The dot/dashed lines are the corresponding projection distances used to reconstruct the trajectory. The ellipses represent the regions near the wires where the field lines make a transition from parallel to radial. The proportions of the ellipses are taken from `GARFIELD` models [14,15].

Electrons ionized by a particle passing through a VDC travel from the trajectory to the sense wires along the path of least time (the arrowed lines). This time is measured by TDCs and converted into a perpendicular distance from the trajectory to the wire plane (the dot/dashed lines). A linear fit is then performed on these drift distances to determine the local cross-over point Qi and local trajectory angle $\theta_{Q\mathrm{i}}$ of the track for each wire plane. Any shortcomings in the conversion algorithm are thus applied identically to each wire. Hence, while the resulting local trajectory angle is a strong function of the conversion algorithm, the local cross-over point is independent of it.

This fact is exploited by performing the particle tracking with a two-VDC system. As shown in Fig. 15, the local cross-over points and wire plane separations d define global trajectory angles Θ_U and Θ_V according to

$$\tan \Theta_Q = \frac{Q2 - Q1}{d}, \tag{4}$$

where $Q \ \epsilon \ (U, V)$. The separation d between like (U1 & U2; V1 & V2) wire planes is approximately 0.335 m. Thus, particle tracking is completely independent of precise knowledge of the local trajectory angles.

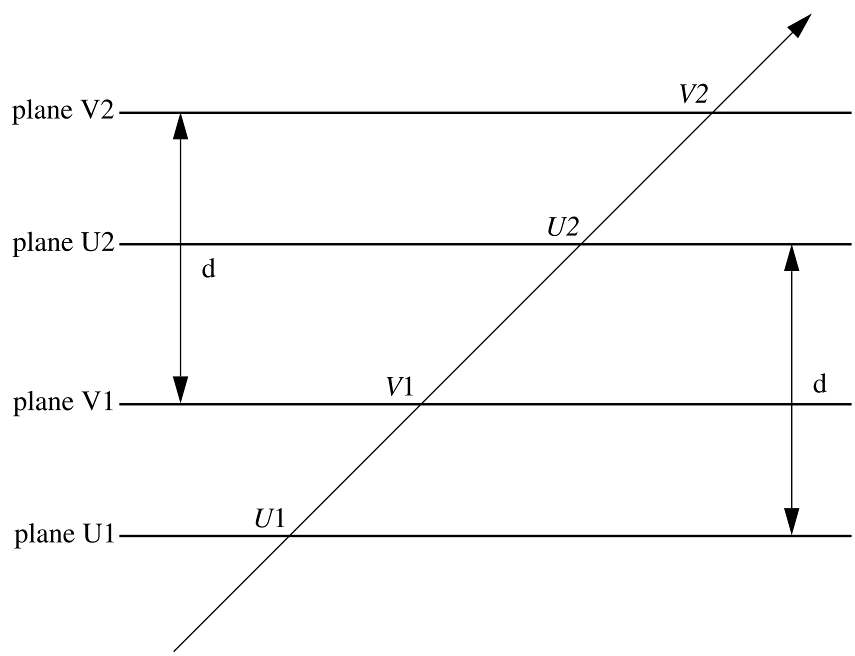

Fig. 15. Trajectory reconstruction for a single track crossing the four wire planes. Note that the U-wires are orthogonal to the V-wires, and that both are oriented at 45° with respect to the plane of the page. The cross-over points are $U1$, $V1$, $U2$, and $V2$. The separation d between like (U1 & U2; V1 & V2) wire planes is approximately 0.335 m.

Fig. 16 shows the geometrical relationship between the coordinates measured by the U1 and V1 planes and the global angles Θ_U and Θ_V.

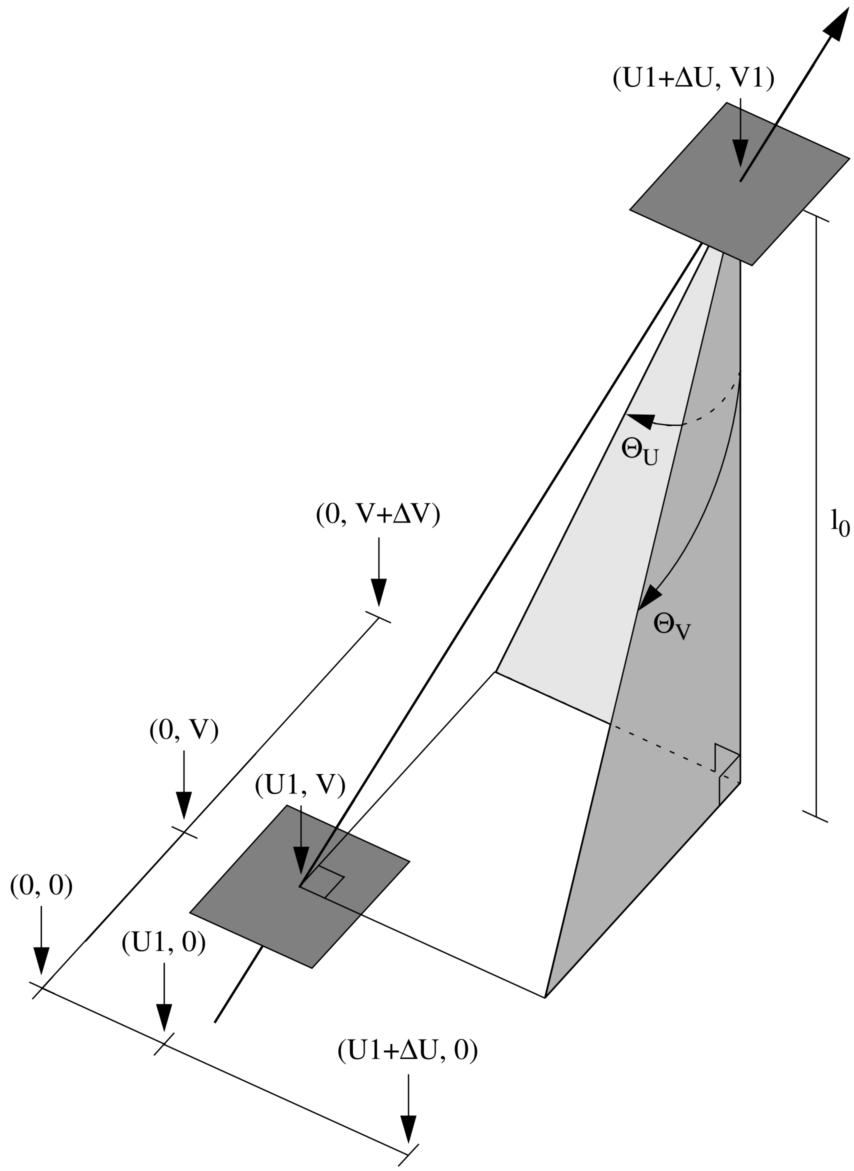

Fig. 16. Geometrical projection of the trajectory coordinates measured by the V1 plane into the U1 plane using the global angles Θ_U and Θ_V.

The global angles are used to project the track coordinate measured by the V1 plane into the U1 plane, according to

$$U = U1, \text{ and} \tag{5}$$

$$V = V1 - \Delta V = V1 - l_0 \cdot \tan \Theta_V. \tag{6}$$

The distance l_0 is the 26-mm perpendicular separation between the U1 and V1 wire planes.

In this manner, every trajectory is categorized with a set of four unique coordinates (U, V, Θ_U, and Θ_V) in a single plane. These coordinates may then be transformed into any number of alternative coordinate systems [21,30].

6.2 Drift times

Fig. 17 shows a typical single-wire drift-time spectrum. These quasielastic data were obtained for a wire located in the center of the focal plane. They correspond to a Gaussian distribution of trajectory angles in the spectrometer midplane with a mean of 45° and a FWHM of 7°. Recall that this corresponds to a mean angle of 55° in the plane perpendicular to the wires.

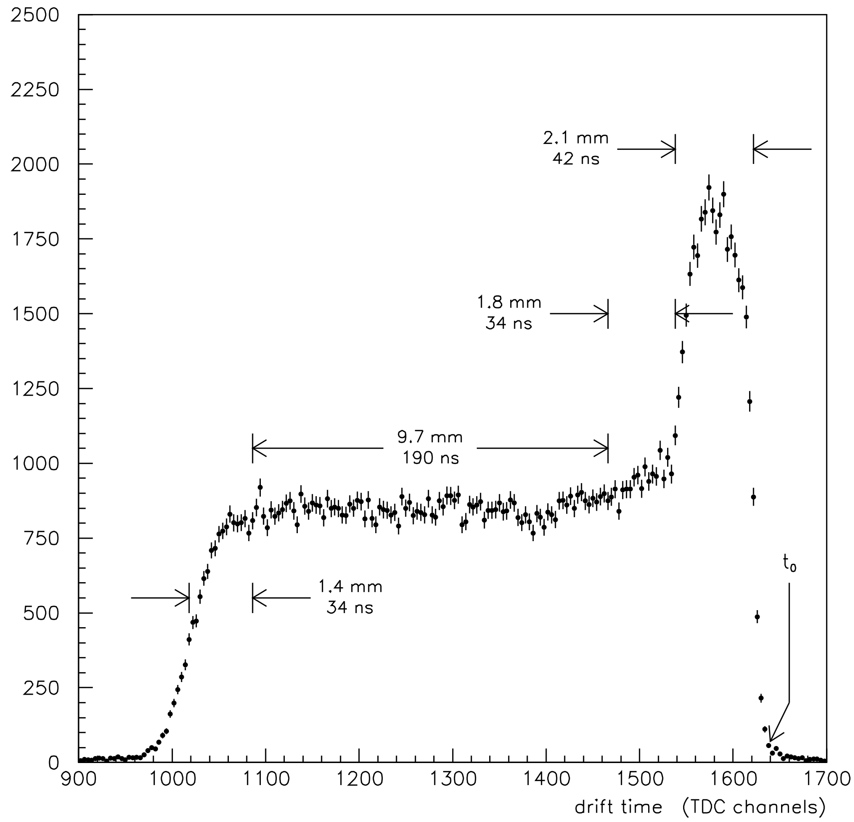

Fig. 17. A single-wire drift-time spectrum. The TDC is operated in common-stop mode, so that short drift times occur at large TDC values. A single time bin is 2.0 ns. The timing reference point t_0 is located at channel 1640.

Because the TDC is operated in common-stop mode, short drift times occur at large TDC values. The shape of the timing spectrum may be understood by considering the typical drift cell and tracks shown in Fig. 18. Here, a uniform illumination is considered, such that the number of trajectories crossing the element of distance dx is given by

$$dN = \text{constant} \cdot dx. \tag{7}$$

In this drift cell, for an element of distance ds along an electric field line, the number of events per time bin $\frac{dN}{dt}$ is

$$\frac{dN}{dt} = \frac{dN}{ds}\frac{ds}{dt}, \tag{8}$$

where $\frac{dN}{ds}$ is the linear density of counts along ds, and $\frac{ds}{dt}$ is the mean drift velocity of the ionization within ds.

In the region near the HV plane, the amount of cell traversed by a particle strongly depends on its track angle. For example, larger trajectory angles intersect a smaller portion of the cell, which results in less total ionization being produced. This in turn reduces the probability of detecting the particle. This geometrical effect leads to a reduction in $\frac{dN}{ds}$ and is evidenced by the shoulder between channels 1020 and 1080 in Fig. 17. The effect takes place in the 1.4 mm region illustrated between the HV plane and track A in Fig. 18.

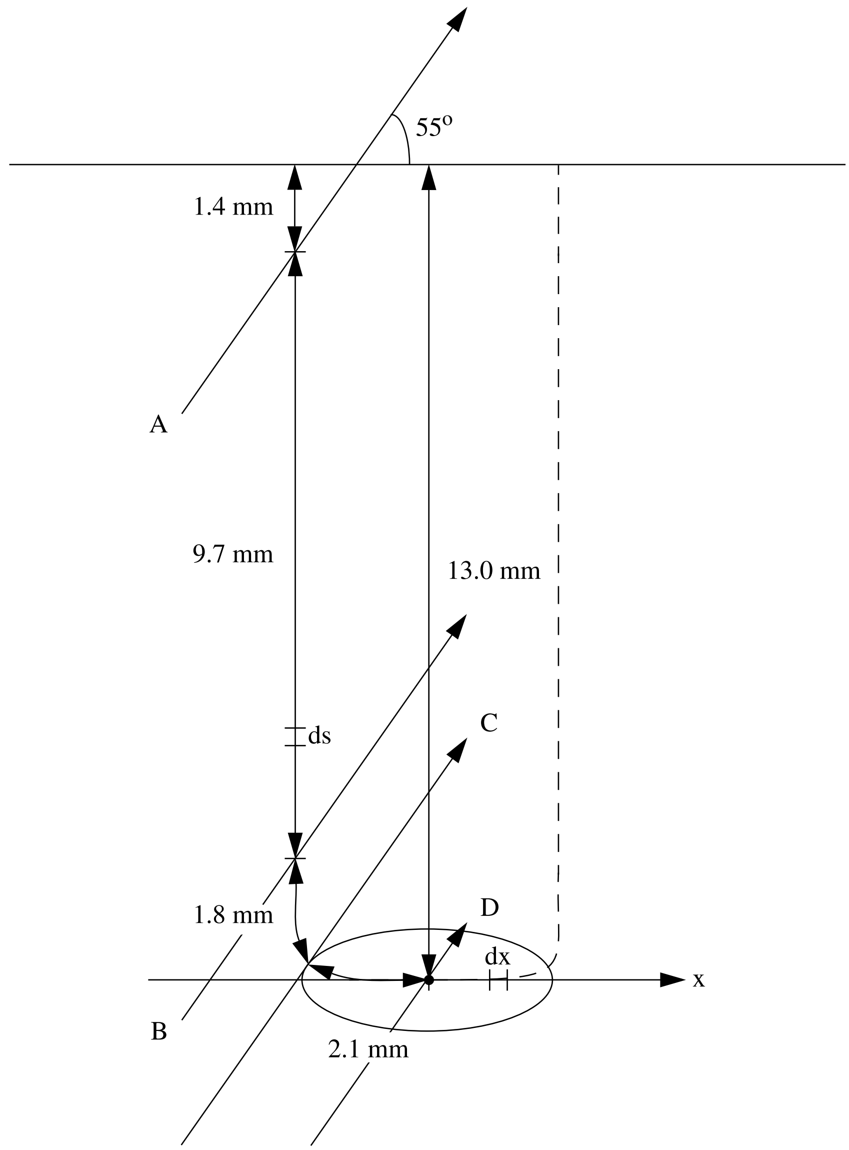

Fig. 18. A drift cell. Extreme field lines are shown. The ellipse represents the region near the wire where the field lines make a transition from constant to quasi-radial. The proportions of the ellipse are taken from the `GARFIELD` model [14,15]. The dimensions correspond to the regions illustrated in Fig. 17. The 55° trajectories illustrated here in the plane perpendicular to the wires represent the mean of the angular distribution of tracks, and correspond to 45° trajectories in the spectrometer midplane.

Over the bulk of the active region of the drift cell, particle tracks cross a zone of purely flat response, where the field lines are parallel and the drift velocity of the liberated ionization electrons is constant. Thus, both $\frac{dN}{ds}$ and $\frac{ds}{dt}$ are constant. This zone corresponds to the flat plateau between channels 1080 and 1460 in Fig. 17 and the 9.7 mm region illustrated between tracks A and B in Fig. 18.

Closer to the sense wire, particle tracks cross a zone where the orientation of the field lines begins to change from parallel to quasi-radial. Thus, while $\frac{ds}{dt}$ remains more or less constant, $\frac{dN}{ds}$ begins to increase. This zone corresponds to the transition region between channels 1460 and 1540 in Fig. 17 and the 1.8 mm region between tracks B and C in Fig. 18.

Finally, in the elliptical region of quasi-radial field near the sense wire, the shape of the drift-time spectrum is due to an interplay between changes in $\frac{dN}{ds}$ (which goes through a maximum) and $\frac{ds}{dt}$ (which begins to rise dramatically, particularly very close to the wire). This zone corresponds to the peak region between channels 1540 and 1620 in Fig. 17 and the 2.1 mm region between tracks C and D in Fig. 18.

To compare drift-time spectra from several wires, timing offsets due to variations in cable lengths and signal processing times must be removed. This is done by systematically calculating a reference timing position (t_0) for the TDC spectrum for each wire and then matching this position in software for all TDC spectra. This common point is located by numerically differentiating the region of short drift times (around channel 1600) channel-by-channel. Once the maximum derivative (the maximum slope of the shoulder) is located and calculated, it is extrapolated to the x-axis. The point of intersection of this line with the x-axis is selected as t_0, which for Fig. 17 is located at channel 1640.

6.3 Drift-time to drift-distance conversion

Numerous algorithms exist for converting drift-time spectra into perpendicular drift-distance spectra [31,32]. One choice of conversion algorithm is outlined below. This algorithm is based entirely upon analysis of actual data obtained using the VDC system.

For a given wire, a spectrum such as Fig. 17 is accumulated. For each time bin t', an integration of the spectrum according to

$$x(t') = \frac{1}{K}\int_{t_0}^{t'} \frac{dN}{dt}dt \qquad (9)$$

converts drift time to drift distance. The result is a lookup table. For completeness, a calibration constant K is selected such that the base width of the drift distance distribution corresponds to the known maximum drift distance within a single drift cell (15.12 mm).

Fig. 19 shows the resulting correspondence between drift time and drift distance obtained from data for VDC plane U1 wire 184 (the central wire). This corresponds to a Gaussian distribution of particle trajectories with a mean angle of 45° and a FWHM of 7° in the spectrometer midplane.

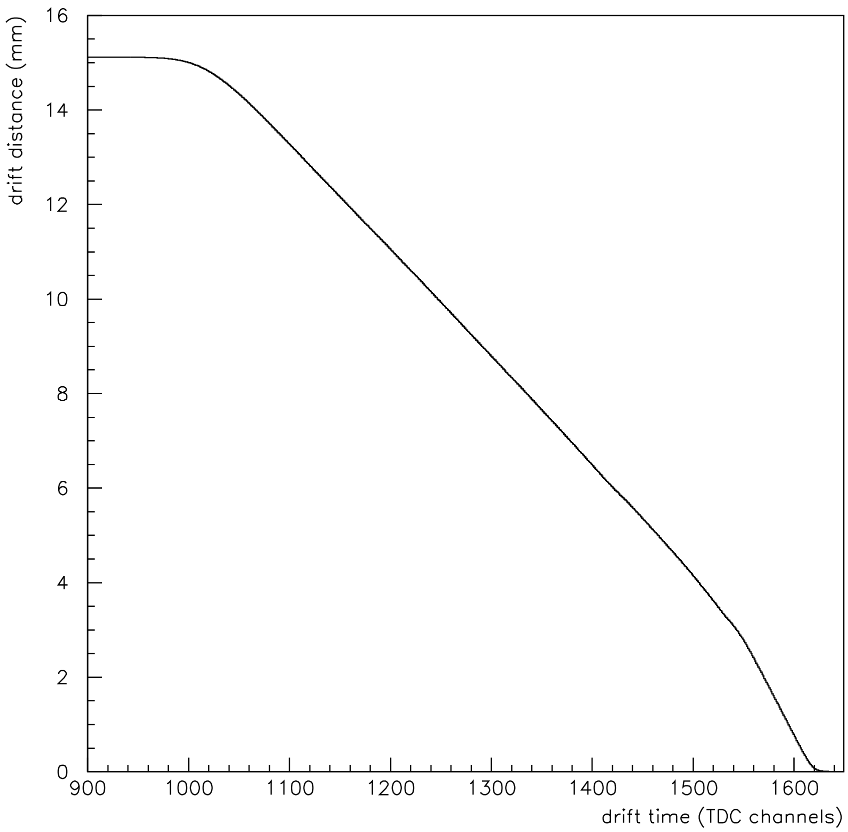

Fig. 19. The correspondence between drift time and drift distance obtained from data for VDC plane U1 wire 184 (the central wire). This corresponds to a Gaussian distribution of particle trajectories with a mean angle of 45° and a FWHM of 7° in the spectrometer midplane. The normalization coefficient K is selected so that the base width of the drift-distance distribution is identical to the known maximum drift distance within a single drift cell. The conversion constant is 0.5 ns per TDC channel.

Fig. 20 shows the drift-distance spectrum extracted from the drift-time spectrum of Fig. 17 using the mapping presented in Fig. 19. As is expected, it is completely flat.

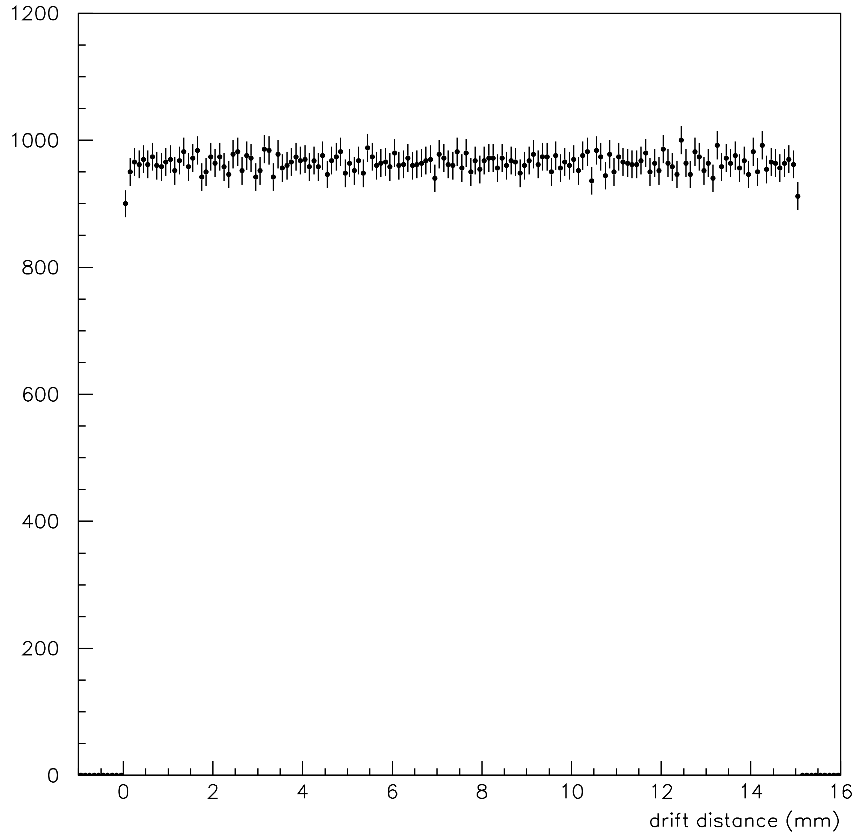

Fig. 20. The drift-distance spectrum corresponding to the drift-time spectrum shown in Fig. 17. The mapping algorithm is the lookup table illustrated in Fig. 19. The bins are 100 μm.

The average track angle of the trajectories changes across the focal plane. By performing the drift-time to drift-distance mapping outlined above for each wire, the correlation between the two quantities may be determined as a function of track angle. This information together with the global trajectory angles (Θ_U and Θ_V, which are constructed from the wire-plane separations d and the local cross-over points Qi), may then be used to perform a precise drift-time to drift-distance conversion corrected for the inclination angle of an individual track at each wire plane.

6.4 Drift velocities

As previously discussed, global trajectory angles are determined by the two-VDC system. From this information, v_{drift}, the characteristic drift velocity of the ionization electrons, was extracted for each VDC.

A single wire in the center of each wire plane was selected. A cut was placed on particle tracks which passed very close to this wire for several trajectory angles. In this manner, 5-cell events with known drift times (and drift distances) which were pairwise equal on either side of the central wire were selected. The TDC spectra for each of the two wires on either side of the selected wire were then examined, and the central values of the distributions determined. On either side of the selected wire, the differences in these central values were calculated. These two differences, necessarily equal, represented the time taken for ionization to drift over a well-defined distance in the region of constant electric field. The ratio of the drift distance to the time difference is the measured drift velocity. The results are presented in Table 2. The error in the values extracted in this manner is approximately 1%.

Table 2
Ionization drift velocities.

wire plane	measured v_{drift} (μm/ns)
U1	50.4
V1	51.1
U2	50.9
V2	50.5

As a check, the local trajectory angles were used to estimate the ionization drift velocity by comparing them to the global trajectory angles on an event-by-event basis. The difference between the two was less than 1%. Also, the computer code `MAGBOLTZ` [33] was used to predict the drift velocity considering the VDC geometry, applied voltage, and gas mixture. The difference between the `MAGBOLTZ`-predicted values and the actual values was less than 3%.

7 Performance

7.1 Operating experience

The VDCs have been in almost continuous use since the beginning of the Hall A EXPINT commissioning program in April 1996. Over this period of time, they have performed in a very reliable fashion. In fact, we have not been able to observe any degradation in wire efficiency over this four-year period.

While we have never been subject to the failure of a gas or HV window, we have incurred a single broken wire. We were able to diagnose the problem and swap in a spare VDC in 24 hours. The subsequent repair of the wire was straightforward and easily achieved due to the single-wire placement technique. The repair procedure (which involved opening the chamber, setting a new wire, closing the chamber, and the subsequent testing) took roughly eight hours of clean room time.

The method of sealing the VDCs has worked sufficiently. None of the VDCs leaks at a rate greater than 3 ℓ/hr, which is within the specified safety requirements. Originally, we had some trouble with the rigidity of the O-rings with respect to our O-ring groove design and bolt placement and obtaining a good seal, but this was overcome by using low-durometer material. In subsequent designs, we will pay closer attention to the mechanics of O-ring placement. We note that if the gas supply to the chambers is interrupted even for periods of up to several hours, the per-wire efficiency remains above 90%.

The mounting frame and support rails have performed flawlessly, with the VDC cartridges being removed and returned to their location in the HRS shielding hut many times. On two occasions known to the authors, the aluminum protective cage has deflected tools accidentally dropped onto it. It has also protected the VDCs from the inescapable welding slag and metal filings generated during upgrades to the shielding houses.

The HV system is very stable. Under normal experimental conditions, with 100 μA of continuous beam on the target (corresponding to a dark current draw of several hundred nA), the average HV trip frequency is about once every 35 000 μA·hours. In real time, this is equivalent to roughly two trips per month.

We have, on several occasions, replaced malfunctioning preamp/discriminator cards. They are often identified by four adjacent wires suddenly going dead, since the cards process signals in a (four wires per chip $\times$ four chips per card) fashion. We have recently observed a gradual increase in the discriminator thresholds we have been forced to use under experimental conditions. We attribute this to the conducting adhesive on the copper tape which is used to anchor the 125-μm sheathing plates drying out with time. The result is poorer contact between the shielding plates, compromising the integrity of the Faraday cage. However, it is easily addressed with maintainence.

Sometimes, during maintainence, we have inadvertantly jarred a conductive bridge between two circuit boards, resulting in electrical isolation of the preamp/-discriminator cards plugged into that board. We simply resolder the bridge.

And finally, the most common problem we have noted is that during routine reinstallation of a VDC cartridge, a few “hot” or “singing” wires are induced by poor connections between the ribbon cables and the TDCs. These are easily identified and taken care of, in most cases simply by wiggling the cable connector at the TDC to improve the connection.

7.2 In-situ resolutions

A thorough optics and resolution commissioning study was performed on the HRS in April 1997, just prior to the commencement of the Hall A EXPINT program. Data taken using the VDCs for (e, e') from a 250-μm thick ^{12}C foil were analyzed to extract the "as-built" optical properties. As a result, in-situ resolutions were extracted and are presented here.

It should be noted that the values quoted in this section are for target variables, and are completely dominated by multiple scattering in the various spectrometer windows. For example, at a scattered electron momentum of 0.845 GeV/c, two 125-μm Kapton windows located approximately 0.5 m from the target contribute 0.8 mrad FWHM, one 100-μm titanium spectrometer exit window located approximately 25.0 m from the target contributes 2.0 mrad FWHM, and roughly 0.325 m of air located between the two VDCs contributes 1.9 mrad FWHM to the overall angular resolution [21]. Thus, in no way do these results reflect the inherent resolution of the VDCs. They are presented to demonstrate the functionality of the chambers. Finally, it should also be noted that the resolution measurements reported here agree well with those predicted by an intensive simulation of the Hall A experiment apparatus [34].

Fig. 21 shows the angular resolution obtained for trajectory angle reconstruction at the target in terms of the laboratory out-of-plane angle θ and in-plane angle ϕ. The data were taken at $E_{\mathrm{beam}} = 0.845$ GeV and $\theta_e = 16°$. These distributions were obtained by placing a cut in software on electrons scattering through the central 2-mm diameter hole of a sieve slit collimator [35] located 1.181 m from the target. They thus represent a convolution of the target width, the hole diameter, and the actual resolutions. The FWHM values (6.0 mrad in θ, 2.3 mrad in ϕ) are for the fitted curves. The overlaid shaded histograms show the results of a simulation which folded a 2.0-mrad FWHM Gaussian distribution (representing the sieve slit hole) with the spectrometer optics and multiple scattering [21]. The agreement is good.

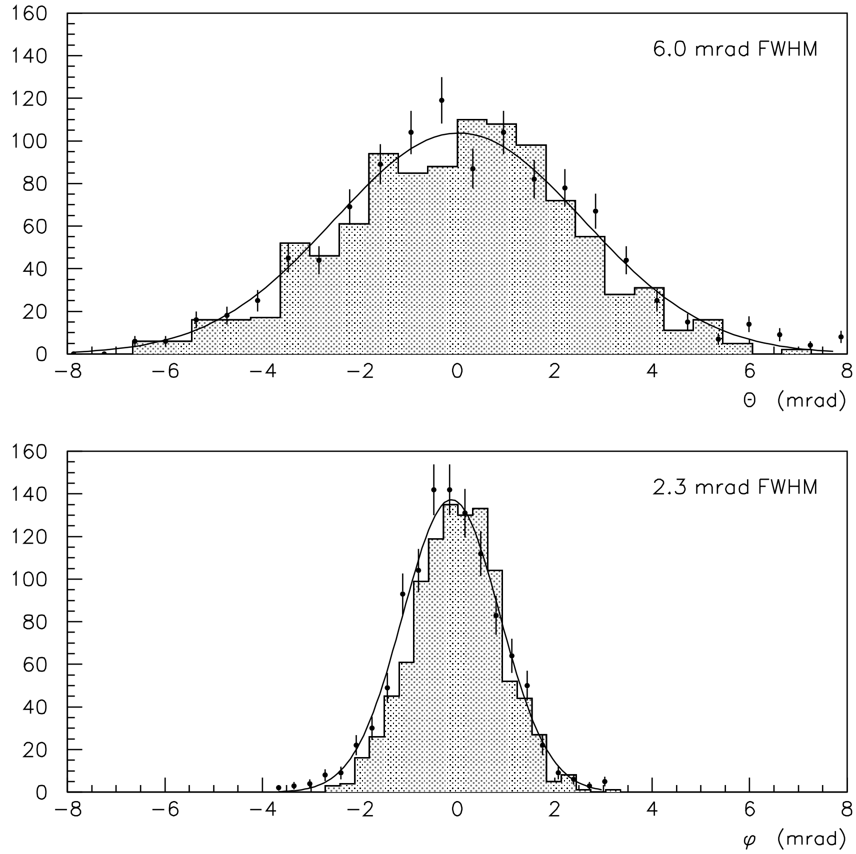

Fig. 21. Angular resolution in θ (the out-of-plane angle) and ϕ (the in-plane angle) obtained for trajectory angle reconstructions at the target. These $^{12}\mathrm{C}(e,e')$ data were taken at $E_{\mathrm{beam}} = 0.845$ GeV and $\theta_e = 16°$. The 250-μm thick target was located 1.181 m from a 2-mm diameter hole in a sieve slit collimator. The distributions thus represent a convolution of the target width, the hole diameter, and the actual resolutions. The FWHM of the fitted curves are 6.0 mrad and 2.3 mrad respectively. The overlaid shaded histograms are for a simulation which folded a 2.0-mrad FWHM Gaussian distribution (representing the sieve slit hole) with the spectrometer optics and multiple scattering [21].

Table 3
In-situ laboratory angular parameters measured by the HRS/VDC system.

angle	FWHM resolution	reconstruction accuracy
out-of-plane (θ)	6.00 mrad	± 0.60 mrad
in-plane (ϕ)	2.30 mrad	± 0.23 mrad

These data have also been analyzed to extract a typical FWHM y_{target} resolution of 1.8 mm and a typcial FWHM momentum resolution $\frac{dP}{P}$ of 2.5×10^{-4} [21].

8 Summary

The High Resolution Spectrometers in Hall A at Jefferson Laboratory have been instrumented with VDCs designed and constructed by the Nuclear Interactions Group at MITLNS in conjunction with the Physics Division at Jefferson Lab. These chambers utilize an individually mounted wire-placement technique, and are unique in that they do not possess any field-shaping wires. They have proven to be very reliable, having been in almost continuous use since April 1996 without any noticeable degradation in per-wire efficiency, providing precision (225 μm FWHM per plane) tracking data for the Hall A physics program.

Acknowledgement

This work was financially supported by the United States Department of Energy. The authors gratefully acknowledge helpful discussions with S. Christo, R. Wojcik (Jefferson Lab) and B. A. Raue (ODU, now at FIU); the courtesy of the Jefferson Lab Hall B CLAS chamber team for sharing their clean room; R. Veenhof (CERN) for assistance with the chamber-simulation program; J. Kelsey (MIT) for advice on mechanical engineering questions; M. Neal, G. Sechen (MIT) and N. Kauffmann, M. Wimbish (Jefferson Lab) for technical support; and MIT undergraduate students for the countless hours they spent stringing the wires for these chambers.

References

[1] http://www.jlab.org/Hall-A

[2] http://www.jlab.org

[3] http://www.jlab.org/Hall-A/equipment/high_resol.html

[4] http://www.jlab.org/Hall-A/physics/experiment_index.html

[5] *Conceptual Design Report, Basic Experimental Equipment,* CEBAF Internal Report (1990); P. E. Ulmer, private communication.

[6] P. E. Ulmer, private communication.

[7] F. Sauli, Principles of Operation of Multiwire Proportional and Drift Chambers, CERN report 77-09, (1977).

[8] W. Bertozzi *et al.*, Nucl. Inst. and Meth. **141**, (1977) 457.

[9] K. I. Blomqvist *et al.*, Nucl. Inst. and Meth. **A403**, (1998) 263.

[10] SLAC, reference to be provided by G. Stephan.

[11] G. Stephan, private communication.

[12] J. A. Kadyk, Nucl. Inst. and Meth. **A300**, (1991) 436.

[13] Stesalit AG Kunststoffwerk, CH-4234 Zullwil SO, Switzerland.

[14] R. Veenhof, Garfield, a drift-chamber simulation program: User's Guide Version 5.18, CERN Technical Memorandom, (1995); http://consult.cern.ch/writeup/garfield/.

[15] R. H. Wechsler, Drift-time Properties of the CEBAF Hall A Vertical Drift Chambers, MIT Undergraduate Thesis (1996).

[16] C. Leathers, Efficiency Measurements on the CEBAF Hall A VDCs, MIT Undergraduate Thesis (1996).

[17] K. G. Fissum, VDC Manual V2.1, MIT Internal Report #03/97 (1997).

[18] http://www.gluguru.com/Structural/Ciba/ciba.html

[19] Luma Metall AB, Box 701, S-391 27 Kalmar, Sweden.

[20] http://www.dupontdow.com/products/viton/default.html

[21] N. Liyanage, Optics Commissioning of the Hall A High Resolution Spectrometers, MIT Internal Report #05/98 (1998).

[22] H. Fenker, Hall A Wire-chamber Gas System (HAWGS) Operations Manual, Hall A Technical Note (1996).

[23] http://www.airproducts.com

[24] M. Atac, IEEE Trans. Nucl. Sci. NS-34 (1) (1987) 476.

[25] `http://www.bertan.com/mwpc.html`,
`http://www.jlab.org/~segal/manuals/bertan/bert_mod.eps`

[26] `http://www.lecroy.com/lrs/`

[27] `http://www.kepcopower.com/ate.htm`

[28] `http://www.kscorp.com`

[29] `http://www.bira.com`

[30] E. A. J. M. Offermann *et al.*, `ESPACE` Manual, Jefferson Lab Technical Memorandum, (1997).

[31] D. Jordan *et al.*, Understanding the Elssy VDC, MIT Internal Report (1992).

[32] D. Jordan, Ph.D. thesis, MIT (1994).

[33] S. F. Biagi, `MAGBOLTZ` computer code, `http://consult.cern.ch/writeup/garfield/help/garfield_22.html#Ref0177`.

[34] E. A. J. M. Offermann *et al.*, The Hall A sextupole crisis: an evaluation of the magnitude of the problem and possible solutions, Jefferson Lab Technical Memorandum (1995).

[35] E. A. J. M. Offermann *et al.*, Nucl. Inst. and Meth. **A262**, (1987) 298.